DOI:10.1039/C2EE00003B (Communication) *Energy Environ. Sci.*, 2012, **5**, 6895-6899

Quartz (SiO_2): a new energy storage anode material for Li-ion batteries†

Won-Seok Chang [a], **Cheol-Min Park** [b], **Jae-Hun Kim** [c], **Young-Ugk Kim** [d], **Goojin Jeong** [c] and **Hun-Joon Sohn** *[a]

[a]*Department of Materials Science and Engineering, Seoul National University, Seoul 151-742, Korea. E-mail: hjsohn@snu.ac.kr; Fax: +82-2-885-9671; Tel: +82-2-880-7226*

[b]*School of Advanced Materials & System Engineering, Kumoh National Institute of Technology, Gumi, 730-701, Korea*

[c]*Advanced Batteries Research Center, Korea Electronics Technology Institute, Seongnam, 463-816, Korea*

[d]*Development Team, Battery Business Division, Samsung SDI, Cheonan, 330-300, Korea*

Received 2nd January 2012 , Accepted 27th February 2012

First published on the web 28th February 2012

SiO_2 is one of the most abundant materials on Earth. It is cost-effective and also environmentally benign when used as an energy material. Although SiO_2 was inactive to Li, it was engineered to react directly by a simple process. It exhibited a strong potential as a promising anode for Li-ion batteries.

Broader context

We are proposing innovative and practical concepts employing facile amorphization of quartz

powders by high energy mechanical milling to obtain high performance anode materials for Li-ion batteries. Silica (SiO_2) is one of the most abundant materials on Earth and the main constituent of sand. It has been known inactive to Li, but was engineered, for the first time, to react directly with Li by simple mechanical milling. Surprisingly, metallic Si and amorphous silicon dioxide as well as gaseous oxygen were evolved from the very stable crystalline silicon dioxide during milling. The size of silicon crystallites was approximately 5 nm and dispersed randomly within the amorphous silicon dioxide matrix. The engineered material reacted with Li exhibiting an excellent electrochemical performance with the capacity of ~800 mA h g^{-1} over 100 cycles without any buffering media when the electrode was subjected to cycling. Also, in spite of the low initial Coulombic efficiency (~37%), we successfully enhanced it up to ~70% by controlling voltage. This process provides a simple, cost-effective and environmentally benign anode material with high capacity for Li-ion batteries.

Introduction

Development of new, safe, low cost and environmentally friendly materials for lithium ion batteries is an essential part of the technological advance of portable electronic devices and electric vehicles. To meet the requirements, such as high capacity, power and stable cycle performance, diverse research has been performed, in the case of the anode, to search for Li-alloying materials with a higher capacity than graphite (LiC_6: 372 mA h g^{-1}).[1] Although alloy systems provide large capacities, *i.e.* Li–Si ($Li_{4.4}Si$: 4198 mA h g^{-1}),[2–4] Li–Sn ($Li_{17}Sn_4$: 959.5 mA h g^{-1}),[5–7] Li–Sb (Li_3Sb: 660 mA h g^{-1})[8,9] and Li–P (Li_3P: 2596 mA h g^{-1}),[10,11] severe cracking and pulverization of electrode materials occur due to a large volume change during the alloying/dealloying with Li. To alleviate this problem, the nanosized or nanostructured materials as well as active/inactive composite materials have been suggested. Nanosized electrode materials can afford to accommodate mechanical strain during cycling. Also, cycle performance could be enhanced by reducing the volume variation that originates from the alloying/dealloying with Li.[12] In the case of Si, it was reported that nanosized Si (78 nm) exhibited a better capacity retention than Si powder (−250 mesh) by Li *et al.*[13] In addition, a reduced diffusion path for ions improved ionic conductivity.[14] There have also been reports of morphology refinement and using favorable structures for the volume variation of Si.[15–17]

Various volume buffering matrices around Li-active materials have been employed to limit the mechanical strain. Carbon has been employed mostly due to its low cost and excellent conductivity.[18–20] Other Li inactive matrices have been tested for elasticity and hardness.[21,22] Even though they presented equivalent problems to carbon, these also offered mechanical rigidity and elasticity to the composite, so that the composite could be robust enough against the stress generated from the volume variation.

Silica (SiO_2) is one of the most abundant materials on Earth, and widely utilized in the glass and electronics industries. However, when applying silica as the anode material for Li secondary batteries, it does not react with Li due to its stability as an oxide. It was reported that it exhibited Li reactivity in amorphous states such as a thin film or hollow sphere,[23–25] but the processes required complex procedures employing high cost precursors. Also the reaction mechanism is not yet clearly understood.

We herein report on the simple, cost-effective and ecologically acceptable material, SiO_2 (quartz), as a precursor, to be used as an anode material for Li secondary batteries by high energy mechanical milling (HEMM).

Experimental

Preparation

HEMM was employed with commercially available SiO_2 (Quartz, Aldrich, −325 mesh) powder. The powder was placed into a hardened steel vial (80 cm^3) with steel balls of two different sizes (3/8 inch, 3/16 inch) at a ball/powder ratio of 20 : 1. The whole apparatus was assembled in an Ar filled glove box. The HEMM process was conducted at 800 rpm.

Materials characterization

Milled SiO_2 samples were characterized by XRD (Rigaku, D-MAX2500). *Ex situ* HRTEM (JEOL 3000F operating at 300 kV) images were obtained at the indicated potential in DCP (Fig. 2b). For the TEM observation, the electrodes were taken off the cell and washed with diethyl carbonate (DEC), and dried in a vacuum chamber. This dilute suspension of the sample was dropped onto a carbon-coated TEM grid and dried in a vacuum chamber for 3 h. Beads were fabricated using LiB for XRF (Bruker S4 Pioneer) analysis. In AES (Perkin-Elmer PHI 660) analysis, sputtering was performed at 3 different sites with a 17 nm min^{-1} rate. FT-IR (Nicolet 6700) analyses were performed in attenuated total reflectance (ATR) mode. For the gas analysis, a steel vial containing

the 24 h milled sample was immersed and opened within a mineral oil (Samchun chemical, Korea) filled container. Bubbles from the vial were collected in a beaker and the gas was captured by a gastight syringe (Hamilton, USA), followed by injecting the samples into a gas-chromatography mass spectrometer (Perkin Elmer Clarus 600T). The injected quantity of each gas (the gas samples from the milling vial and glove box) was 200 μl. Each run was performed for 15 min.

Electrochemical measurements

Electrodes were fabricated for the electrochemical evaluation. Pristine and milled SiO_2 samples (70 wt%) were mixed with *N*-methyl pyrrolidinone (NMP) (solvent), polyamide imide (15 wt%, binder, Solvay) and Ketchen black (15 wt%, conducting agent) at 55 ℃. The slurries were coated on copper foil and dried under vacuum at 200 ℃ for 4 h. Coin-type cells were assembled in an Ar-filled glove box using Celgard 2400™ as the separator. Li foil was used as the counter and reference electrodes. 1 M $LiPF_6$ in ethylene carbonate (EC)/diethyl carbonate (DEC) (3 : 7 by volume) and 10% fluoroethylene carbonate (Panax Starlyte) was used as the electrolyte. Cells were tested galvanostatically between 0.0 and 2.0 V (*vs.* Li/Li^+) at a current of 100 mA g^{-1}. In the case of voltage control, the potential was lowered to 0.27 V and held for 24 h, then followed by a charging step at the 1^{st} cycle only. Li was inserted while the cell was discharging and was extracted during charging.

Results and discussion

Pristine SiO_2 (Aldrich, −325 mesh), a main constituent of sand, and 24 h milled samples (<300 nm) were characterized by using an X-ray diffractometer (XRD), and they are compared in Fig. 1a and b (SiO_2 samples with different milling times are illustrated in Fig. S1a†). All the characteristic peaks corresponding to crystalline SiO_2 vanished and the peaks were broadened, revealing an amorphous nature, with a further increase in milling time. A Fourier transform infrared spectrophotometer (FT-IR) was employed in the absorbance mode, and the spectra are compared in Fig. 1c. In the case of the 24 h milled sample, broadening of the full width at half-maximum (FWHM) of the Si–O stretching peak could be noticed, and a red shift (1056 cm^{-1} to 1018 cm^{-1}) of frequency occurred. The red shift phenomenon due to amorphization was also observed by Liu *et al.*,[26] in which the Si stretching peak of the amorphous state shifted to a lower position and the FWHM became narrow after annealing. This result agrees well with our result. FT-IR spectra with

different HEMM operation hours are given in Fig. S1b†.

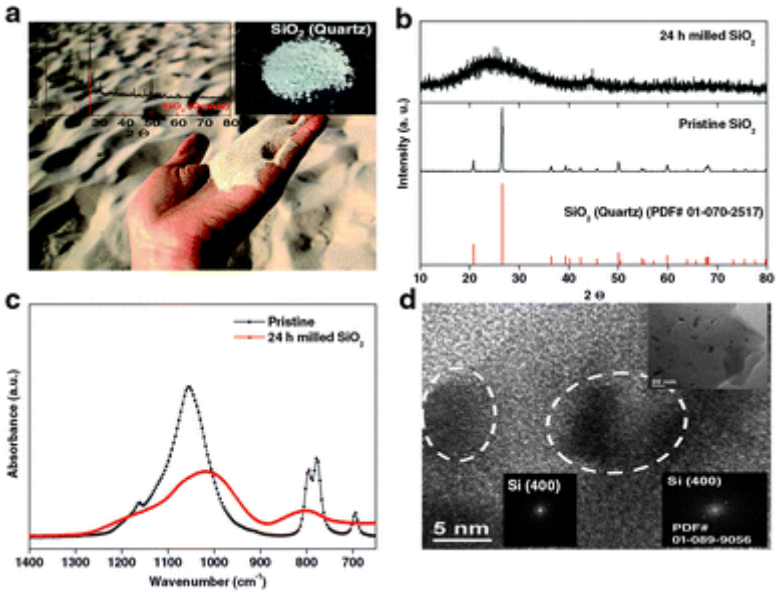

Fig. 1 (a) Beach sand with XRD pattern and pristine silica powder (upper right). (b) XRD patterns, (c) FT-IR spectra and (d) HRTEM image of 24 h milled SiO_2, respectively.

In order to observe the microstructural change during milling, a high resolution transmission electron microscope (HRTEM) was employed, and the image for 24 h milled sample is shown in Fig. 1d. SiO_2 had started to be amorphized in the case of the 12 h milled sample but, unexpectedly, Si crystallites of nanometre size (~5 nm) were observed in the 24 h milled sample (12 and 36 h samples are shown in Fig. S2a and S2b†, respectively). This indicated that the O/Si ratio of the milled SiO_2 samples should be decreased; thus, X-ray fluorescence (XRF) spectrometry and Auger electron microscopy (AES) with a depth profile (to 200 nm) for the solid phase (quantitative) as well as gas chromatography (GC) for gas phase analyses (qualitative) were carried out. Tests were performed three times for each sample. The average ratios of O/Si, based on XRF data, were 1.9997, 1.989, 1.929 and 1.935 for pristine SiO_2, 12 h, 24 h and 36 h milled SiO_2 samples, respectively. Also according to the AES profiles, pristine SiO_2 exhibited a consistent ratio (oxygen

to Si) of 2.0, while the average O/Si ratio for 42 points along a channel of 200 nm depth in the 24 h milled SiO_2 sample was ~1.91, which compared with 1.93 from the XRF data. The oxygen concentration in the gas phase in the vial during milling for the 24 h milled SiO_2 sample was dramatically increased compared to that of the Ar sample, taken from the Ar filled glove box as illustrated in Fig. S3†. This result explained the evolution of a small amount of nanosize Si crystallites (~2.15 wt%) in the amorphous SiO_2 phase, and also confirmed the AES and XRF data mentioned above. The oxide reduction by the HEMM was also observed by Jung *et al.* using MoO_3 oxide.[27]

Preliminary experiments showed that the 24 h milled SiO_2 sample showed the best electrochemical performance among the three samples, and the electrochemical behaviors of the 24 h milled SiO_2 sample were analyzed in detail. Fig. 2a shows the voltage profile of the 24 h milled SiO_2 sample at the 1st and 10th cycles. The discharge and charge capacities of the 1st cycle were 2243 and 827 mA h g^{-1}, respectively, with a low initial Coulombic efficiency of 37%. The corresponding differential capacity plots (DCPs) are illustrated in Fig. 2b. A large surge in the profile was detected at 0.22 V during the first discharging step, but this did not occur during the second cycle. This was caused, in general, by the large overpotential associated with the metal oxide electrode during the reaction with Li.[28]

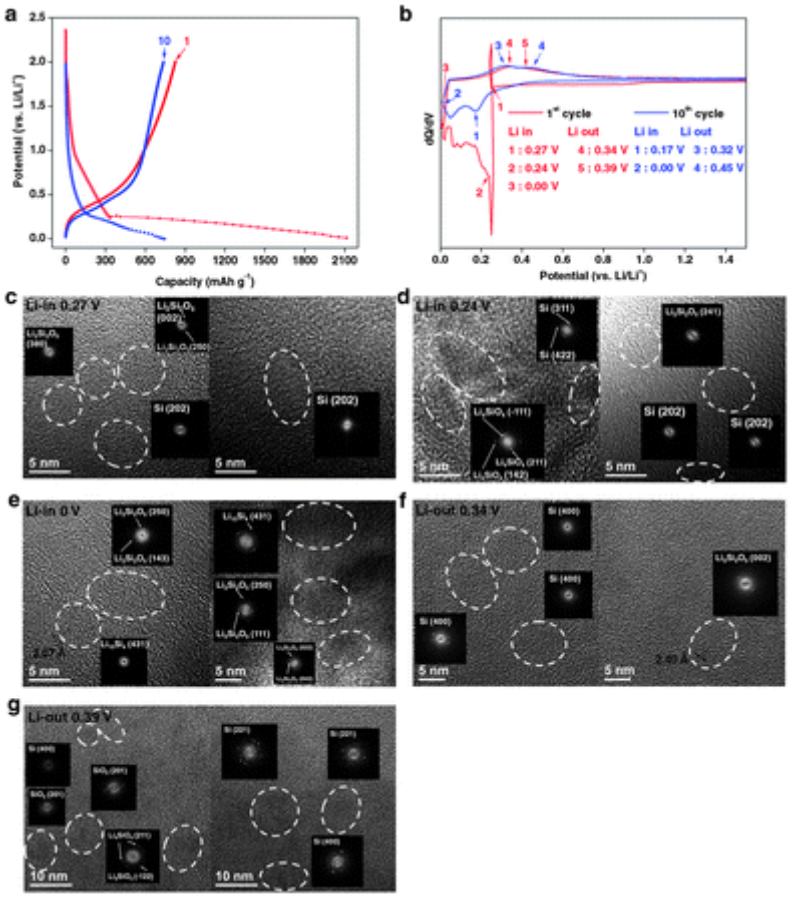

Fig. 2 (a) Voltage profile of 24 h milled SiO_2 at the 1st and 10th cycles. (b) Differential capacity plot (DCP) of 24 h milled SiO_2 (at the 1st and 10th cycles). *Ex situ* HRTEM images (c) discharge at 0.27 V, (d) discharge at 0.24 V, (e) discharge at 0.0 V, (f) charge at 0.34 V and (g) charge at 0.39 V, respectively.

The SiO_2 (α-quartz) consisted of a 144 °bond angle of Si–O–Si, which indicated 6-membered rings. The thermally grown oxide on the Si substrate also mainly consisted of a 144 °bond angle of Si–O–Si with a smaller population of bond angles of 120 °(4-membered rings) and 160 °or more (7-, 8-membered rings).[29] When this oxide on the Si substrate was bombarded with static defocused He^+ ion beams, the bond angles were widely redistributed into 4-membered rings as well as 7- and 8-membered rings.[29] Such a change of the bridging bond angle occurred not only in

the presence of new chemical species but also during local atomic rearrangement (geometry), and could induce a valence charge redistribution, causing the core-level binding energies to shift (chemical shift).[30] The binding energy of each Si 2p and O 1s level in the network was directly dependent on the structure of the network,[31] and atomic rearrangement from the crystalline to amorphous state would occur due to repeated impacts during the HEMM process. The structural transformation may lead to the change in the valence charge, and this could be related to the Li-reactivity of milled amorphous SiO_2 similar to that of SiO consisting of various valence states of Si,[32,33] while crystalline quartz did not react with Li.

To identify the reaction mechanism, since no distinguishable peaks in the XRD patterns were observed, *ex situ* HRTEM images were obtained at selected potentials indicated in the DCPs, and the results are shown in Fig. 2c–g. When the potential was lowered to 0.27 V, unreacted Si and $Li_2Si_2O_5$ phases appeared (Fig. 2c). At 0.24 V, another Li silicate, Li_4SiO_4, also formed (Fig. 2d). As the potential reached 0.0 V, the $Li_{15}Si_4$ phase was observed, as shown in Fig. 2e. Among the above Li-silicates, it was noted that the formation of the $Li_2Si_2O_5$ phase was reversible for the SiO_2 thin film anode,[23] while the Li_4SiO_4 formed during synthesis of the SiO_x/C composite was irreversible[34] during cycling. When Li was extracted during charging, decomposition of $Li_{15}Si_4$ was observed at 0.34 V (Fig. 2f). Upon further charging, Si nanocrystallites, SiO_2 and Li_4SiO_4 phases were detected at 0.39 V (Fig. 2g).

Based on the HRTEM results, the reaction with Li during the 1st cycle can be expressed as follows (a-SiO_2 = amorphous SiO_2),

Discharge reaction

• 0.27 V

$$\text{a-SiO}_2 + (4/5)\text{Li}^+ + (4/5)\text{e}^- \rightarrow (2/5)\text{Li}_2\text{Si}_2\text{O}_5 + (1/5)\text{Si} \quad (1)$$

• 0.24 V

$$\text{a-SiO}_2 + 2\text{Li}^+ + 2\text{e}^- \rightarrow (1/2)\text{Li}_4\text{SiO}_4 + (1/2)\text{Si} \quad (2)$$

• 0.0 V

$$\text{Si} + (15/4)\text{Li}^+ + (15/4)\text{e}^- \rightarrow (1/4)\text{Li}_{15}\text{Si}_4 \quad (3)$$

Charge reaction

• 0.34 V

$$Li_{15}Si_4 \rightarrow 15Li^+ + 4Si + 15e^- \quad (4)$$

• 0.39 V

$$Li_2Si_2O_5 + (1/2)Si \rightarrow (5/2)SiO_2 + 2Li^+ + 2e^- \quad (5)$$

In reaction (3), Si released from the above reactions (1) and (2), as well as that evolved during the milling, reacted with Li at this potential. In the 10th cycle, reversible phases such as $Li_{15}Si_4$ and $Li_2Si_2O_5$ were repeatedly formed and decomposed into Si and SiO_2, respectively (Fig. S4†).

The crystalline structures of reversible $Li_2Si_2O_5$ (S.G. *Ccc*2, *a* = 5.807 Å, *b* = 14.582 Å, *c* = 4.773 Å) and irreversible Li_4SiO_4 phases (S.G. *P*121/*M*1, *a* = 5.147 Å, *b* = 6.094 Å, *c* = 5.293 Å) are illustrated in Fig. 3a. The *b*-axis length of the unit cell for orthorhombic $Li_2Si_2O_5$ is 2.4 times longer (14.582 Å) than that of monoclinic Li_4SiO_4 (6.094 Å). The open tunnel structure along the *c*-axis in the $Li_2Si_2O_5$ phase could provide easy diffusion paths for Li ions, a fact which supported the reversibility of the $Li_2Si_2O_5$ phase.

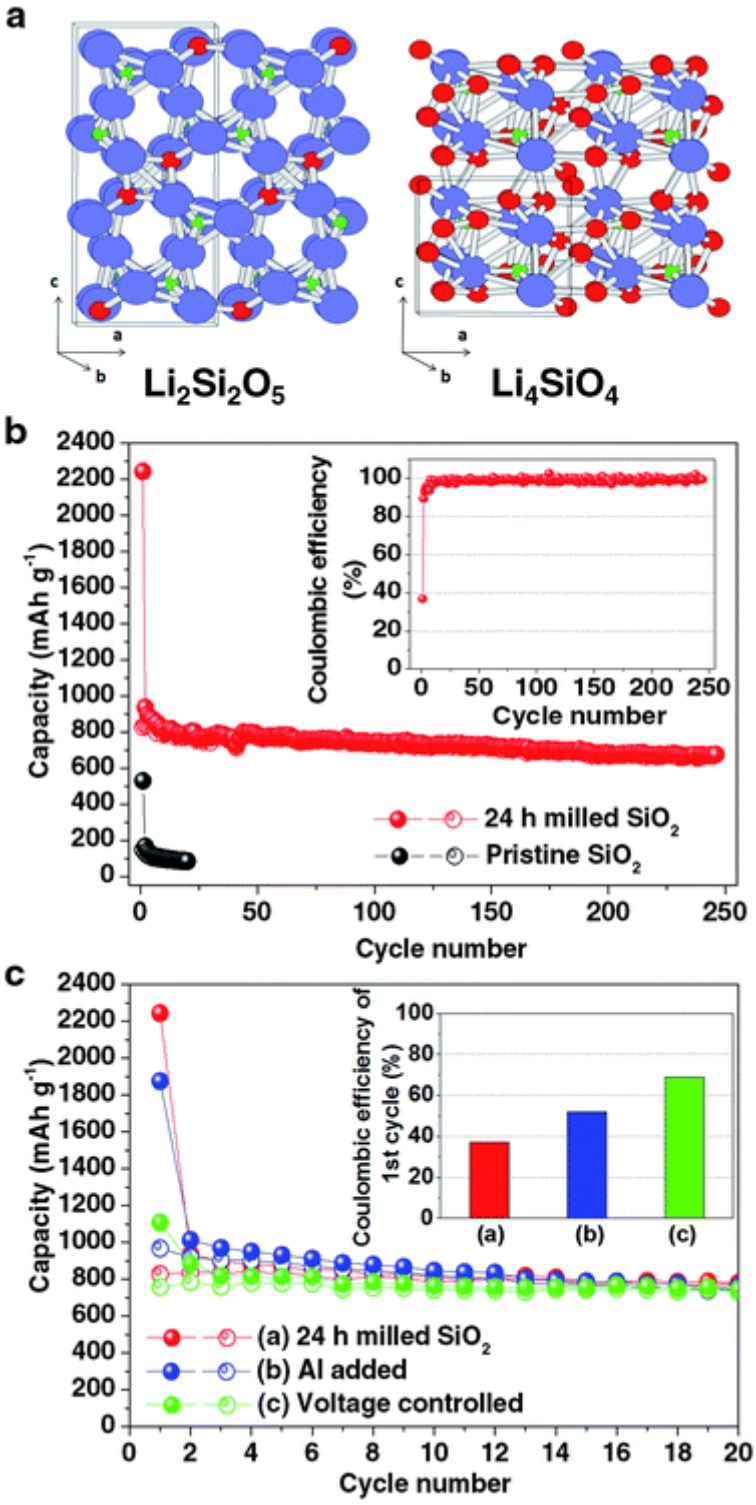

Fig. 3 (a) Ball–stick models of crystal structures of $Li_2Si_2O_5$ and Li_4SiO_4 (red: lithium, green: silicon, purple: oxygen). (b) Comparison of cycle performance between pristine and 24 h milled SiO_2 (inset: Coulombic efficiency over

200 cycles). (c) Cycle performance of Al added and voltage controlled SiO_2 samples (inset: increasing tendency of Coulombic efficiency due to the addition of metal (b) or voltage control (c)).

Cycle performances of pristine and 24 h milled samples are compared in Fig. 3b. Cycle performances with different HEMM operation times are also given in Fig. S5†, and 12 h milled SiO_2 exhibited a negligible reactivity with Li. On the other hand, reversible Li insertion and extraction were observed for the 24 h and 36 h milled SiO_2 samples. In the case of the 24 h milled sample, the drastic decrease of the charge capacity compared to the discharge capacity during the 1st cycle was attributed to the formation of an irreversible Li silicate (Li_4SiO_4) (~928 mA h g^{-1}) and some of the Li remained in the conducting agent (~488 mA h g^{-1}). Although 24 h milled SiO_2 showed a low initial Coulombic efficiency of 37%, it was recovered to ~99% from the next cycle as illustrated in the inset. Furthermore, the capacity retention of the electrode was ~90% at the 100th cycle and over 80% over 200 cycles.

Fig. 3c shows the cycle performances of Al added (15 wt%) and voltage controlled SiO_2, respectively. Addition of Al metal, which can reduce the SiO_2 during milling, could enhance the initial efficiency from 37% to 52%. Also, controlling the voltage down to 0.27 V to form the reversible $Li_2Si_2O_5$ phase only at the 1st cycle was suggested to increase the initial Coulombic efficiency. It is a similar concept to the memory effect.[35] In this case, the initial Coulombic efficiency was dramatically enhanced to ~70%. Both methods did not affect the cycle performance.

Since the amount of metals added, the voltage control, and the operating conditions of HEMM would significantly affect the electrochemical performance, these factors should be optimized to increase the 1st cycle Coulombic efficiency.

Conclusions

In conclusion, we have fabricated, for the first time, nanosized Si embedded in amorphous silica using bulk crystalline quartz (SiO_2) powders through a HEMM method. When applied as an anode material in Li-ion batteries, the 24 h milled SiO_2 exhibited a reversible capacity of ~800 mA h g^{-1} over 200 cycles. The advantages of the milled SiO_2 anode material designed here include its low cost for mass production, the abundance of raw material, and its high reversible capacity with excellent cyclability. These advantages could trigger further research for commercialization of silica based high performance anodes for Li-ion batteries.

Acknowledgements

This work was supported by the research fund of the POSCO Chair Professor (H.-J. Sohn) at the Seoul National University.

Notes and references

1 J. R. Dahn, T. Zheng, Y. Liu and J. S. Xue, *Science*, 1995, **270**, 590–593 CAS Search PubMed.

2 C. J. Wen and R. A. Huggins, *J. Solid State Chem.*, 1981, **37**, 271–278 CrossRef CAS Search PubMed.

3 T. D. Hatchard and J. R. Dahn, *J. Electrochem. Soc.*, 2004, **151**, A838–A842 CrossRef CAS Search PubMed.

4 Y. Idota, T. Kubota, A. Matsufuji, Y. Maekawa and T. Miyasaka, *Science*, 1997, **276**, 1395–1397 CrossRef CAS Search PubMed.

5 C. J. Wen and R. A. Huggins, *J. Electrochem. Soc.*, 1981, **128**, 1181–1187 CrossRef CAS Search PubMed.

6 L. Y. Beaulieu, T. D. Hatchard, A. Bonakdarpour, M. D. Fleischauer and J. R. Dahn, *J. Electrochem. Soc.*, 2003, **150**, A1457–A1464 CrossRef CAS Search PubMed.

7 J.-M. Lee, W.-S. Chang, B. C. Yu, H. Kim, D. Im, S.-G. Doo and H.-J. Sohn, *Electrochem. Commun.*, 2010, **12**, 928–932 CrossRef CAS Search PubMed.

8 C.-M. Park and H.-J. Sohn, *Chem. Mater.*, 2008, **20**, 6319–6324 CrossRef CAS Search PubMed.

9 C.-M. Park and H.-J. Sohn, *Adv. Mater.*, 2010, **22**, 47–52 CrossRef CAS Search PubMed.

10 D. C. S. Souza, V. Pralong, A. J. Jacobson and L. F. Nazar, *Science*, 2002, **296**, 2012–2015 CrossRef CAS Search PubMed .

11 C.-M. Park and H.-J. Sohn, *Adv. Mater.*, 2007, **19**, 2465–2468 CrossRef CAS Search PubMed .

12 W.-R. Liu, Z.-Z. Guo, W.-S. Young, D.-T. Shieh, H.-C. Wu, M.-H. Yang and N.-L. Wu, *J. Power Sources*, 2005, **140**, 139–144 CrossRef CAS Search PubMed .

13 H. Li, X. Huang, L. Chen, Z. Wu and Y. Liang, *Electrochem. Solid-State Lett.*, 1999, **2**, 547–549 CrossRef CAS Search PubMed .

14 A. S. Arico, P. Bruce, B. Scrosasti, J. M. Tarascon and W. Schalkwijk, *Nat. Mater.*, 2005, **4**, 366–377 CrossRef CAS Search PubMed .

15 M. H. Park, M. G. Kim, J. B. Joo, K. T. Kim, J. Y. Kim, S. H. Ahn and J. P. Cho, *Nano Lett.*, 2009, **9**, 3844–3847 CrossRef CAS Search PubMed .

16 H. S. Choi, J. G. Lee, H. Y. Lee, S. W. Kim and C. R. Park, *Electrochim. Acta*, 2010, **56**, 790–796 CrossRef CAS Search PubMed .

17 Y. S. Jung, K. T. Lee and S. M. Oh, *Electrochim. Acta*, 2007, **52**, 7061–7067 CrossRef CAS Search PubMed .

18 J.-H. Kim, H.-J. Sohn, H. Kim, G. Jeong and W. Choi, *J. Power Sources*, 2007, **170**, 456–459 CrossRef CAS Search PubMed .

19 C.-M. Park, Y.-U. Kim, H. Kim and H.-J. Sohn, *J. Power Sources*, 2006, **158**, 1451–1455 CrossRef CAS Search PubMed .

20 Y. Liu, K. Hanai, J. Yang, N. Imanishi, A. Hirano and Y. Takeda, *Electrochem. Solid-State Lett.*, 2004, **7**, A369–A372 CrossRef CAS Search PubMed .

21 G. Jeong, Y.-U. Kim, H.-J. Sohn and T. Kang, *J. Power Sources*, 2001, **101**, 201–205 CrossRef CAS Search PubMed .

22 H. Jung, Y.-U. Kim, M. S. Sung, Y. Hwa, G. Jeong, G. B. Kim and H.-J. Sohn, *J. Mater. Chem.*, 2011, **21**, 11213–11216 RSC .

23 Q. Sun, B. Zhang and Z.-W. Fu, *Appl. Surf. Sci.*, 2008, **254**, 3774–3779 CrossRef CAS Search PubMed .

24 B. Guo, J. Shu, Z. Wang, H. Yang, L. Shi, Y. Liu and L. Chen, *Electrochem. Commun.*, 2008, **10**, 1876–1878 CrossRef CAS Search PubMed .

25 M. Sasidharan, D. Liu, N. Gunawardhana, M. Yoshio and K. Nakashima, *J. Mater. Chem.*, 2011, **21**, 13881–13888 RSC .

26 Y. Liu, T. P. Chen, Y. Q. Fu, M. S. Tse, J. H. Hsieh, P. F. Ho and Y. C. Liu, *J. Phys. D: Appl. Phys.*, 2003, **36**, L97–L100 CrossRef CAS Search PubMed .

27 Y. S. Jung, S. K. Lee, D. J. Ahn, A. C. Dillon and S. H. Lee, *J. Power Sources*, 2009, **188**, 286–291 CrossRef CAS Search PubMed .

28 H. Wang, L.-F. Cui, Y. Yang, H. S. Casalongue, J. T. Robinson, Y. Liang, Y. Cui and H. Dai, *J. Am. Chem. Soc.*, 2010, **132**, 13978–13980 CrossRef CAS Search PubMed .

29 T. Ajioka and S. Ushino, *Appl. Phys. Lett.*, 1986, **48**, 1398–1399 CrossRef CAS Search PubMed .

30 F. J. Grunthaner, P. J. Grunthaner, R. P. Vasquez, B. F. Lewis and J. Maserjian, *Phys. Rev. Lett.*, 1979, **43**, 1683–1686 CrossRef CAS Search PubMed .

31 S. Hofmann and J. H. Thomas, III, *J. Vac. Sci. Technol., B*, 1983, **1**, 43–47 CAS Search PubMed .

32 K. Schulmeister and W. Mader, *J. Non-Cryst. Solids*, 2003, **320**, 143–150 CrossRef CAS Search PubMed .

33 C.-M. Park, W. Choi, Y. Hwa, J.-H. Kim, G. Jeong and H.-J. Sohn, *J. Mater. Chem.*, 2010, **20**, 4854–4860 RSC .

34 A. Veluchamy, C. H. Doh, D. H. Kim, J. H. Kim, D. J. Lee, K. H. Ha, H. M. Shin, B. S. Jin, H. S. Kim, S. I. Moon and C. W. Park, *J. Power Sources*, 2009, **188**, 574–577 CrossRef CAS Search PubMed .

35 D. Linden, in *Handbook of Batteries*, ed. T. B. Reddy, McGraw-Hill, New York, 3rd edn, 2002 .

Footnote

† Electronic supplementary information (ESI) available. See DOI: 10.1039/c2ee00003b

---